Environmental Processes (2024) 11:38
https://doi.org/10.1007/s40710-024-00715-5

RESEARCH

Synthesis of $NaAlSiO_4$ Hollow Microspheres as Absorbents for the Removal of Heavy Metal Ions from Wastewater

Zhiyuan Ouyang[1] · Lihui Meng[1] · Yanru Hu[1] · Wenchao Li[1] · Fang Zhu[1] · Bin Xie[1] · Zilin Zhou[1] · Shuojie Cui[1] · Meng Wang[1] · Qingzhi Wu[1]

Received: 12 December 2023 / Accepted: 1 July 2024

Abstract
In this study, $NaAlSiO_4$ hollow microspheres for Ni(II) and Cd(II) removal from wastewater were synthesized through a solvothermal method combined with calcination treatment. The hollow microspheres were characterized by SEM, TEM, DSC, XRD, FT-IR, and N_2 adsorption/desorption analyzer. The average diameter of microspheres was approximately 2 ± 0.5 μm, and the average pore size was approximately 20 ~ 60 nm. The removal ability was evaluated under different conditions, including various pH values, metal ion concentrations, and adsorption times. Results show that the adsorption capacity of the $NaAlSiO_4$ hollow microspheres depends on the surface area and the content of hexadecyl trimethyl ammonium bromide for Ni(II) and Cd(II), respectively. The maximum adsorption capacity calculated from Langmuir models was 297.11 mg/g for Ni(II) and 449.71 mg/g for Cd(II). The adsorption isotherm and kinetic fitting preferably agree with the Langmuir isotherm model with monolayer coverage. The Ni(II) adsorption efficiency was still more than 95% (Cd(II) adsorption efficiency significantly decreased to 23%) after four cycles, suggesting the high reusability of the hollow microspheres for Ni(II). The successful removal of Ni(II) and Cd(II) from water samples demonstrates the great potential of the proposed $NaAlSiO_4$ to remediate Ni(II) and Cd(II) polluted water in environmental remediation.

Keywords $NaAlSiO_4$ · Hollow microspheres · Heavy metal ions · Environmental remediation

Zhiyuan Ouyang and Lihui Meng contributed equally to this work.

✉ Qingzhi Wu
wuqzh@whut.edu.cn

[1] State Key Laboratory of Advanced Technology for Materials Synthesis and Processing, Wuhan University of Technology, Wuhan 430070, P. R. China

Published online: 10 July 2024

1 Introduction

Heavy metal ions are discharged into water through metal smelting and processing (Adnan et al. 2022), discharge of chemical wastewater (Damiri et al. 2022; Kusworo et al. 2021; Velusamy et al. 2021), abuse of pesticides and fertilizers (Khatun et al. 2022), and disposal of domestic garbage (Guo et al. 2022b; Lv et al. 2022), causing serious pollution to the environment and serious harm to human health. Ni(II) and Cd(II) are two of the most common heavy metal ions found in effluents from a wide range of industries, which have been identified as the most dangerous heavy metals. Both are non-biodegradable and easily enriched in organisms and can cause various serious diseases, such as kidney damage, bone degeneration, hypertension, emphysema, nervous system damage, and even cancer(Beniamino et al. 2022; Thévenod and Lee 2013). The Studies have shown that the maximum Ni(II) and Cd(II) in drinking water are 20 μg/L and 3.0 μg/L(Islam et al. 2019; Sheikh et al. 2023). Therefore, in order to protect water quality and human health, efficient technology is urgently needed to remove excessive Ni(II) and Cd(II) in water. In recent years, many effective methods for removing heavy metal ions have been developed, including chemical precipitation (Benalia et al. 2021; Hu et al. 2021), ion exchange(Ahmad et al. 2021), adsorption (Guo et al. 2022b), membrane filtration (Kusworo et al. 2021), oxidation–reduction (Song et al. 2022), and biological and photocatalytic methods(Punia et al. 2022; Razzak et al. 2022). Among these methods, the adsorption method is widely used due to its simple, effective, and low-cost treatment (Guo et al. 2022b; Mao and Gao 2021). Adsorption strategies mainly include physical adsorption and chemical adsorption. Several types of adsorbents, including natural wastes, polymers, metal nanoparticles, metal oxide nanoparticles, carbon-based nanomaterials and ligand based composite materials have been used (Awual 2019; Awual et al. 2020; Dou et al. 2019a, b; Liu et al. 2019; Salman et al. 2023; Waliullah et al. 2023). However, in large-scale practical applications, conventional adsorbents still have problems such as high cost, difficult production methods, and low reusability. The search for efficient and inexpensive Cd(II) adsorbent materials is an effective way to solve the problem of Cd(II) pollution.

The high surface area, large interior space, and good thermal and mechanical properties of hollow microspheres make it a better adsorbent compared to conventional materials (An et al. 2017; Gong et al. 2014). Various kinds of microspheres can be used for heavy metal ion adsorption, such as glass microspheres, metal microspheres, ceramic microspheres, etc. (Monier et al. 2010; Rostamian et al. 2011; Tang et al. 2022). Recently, mesoporous ceramic hollow microspheres have attracted considerable attention due to their good performance, such as low cost, minimization of secondary wastes, large surface area, and high mechanical stability (An et al. 2020; Qiao et al. 2022; Samad et al. 2021; Yan et al. 2019). The hollow interior space is created either by dissolution of the core using a suitable solvent or by calcination at high temperature. Microspheres can be manufactured by different production methods and have their own unique functions and structures. At present, the commonly used production methods of hollow microspheres include the sol-gel method (Wang et al. 2022a), solvothermal method (Jin et al. 2022), hydrothermal method (Vereshchagina et al. 2018), spray drying method (Qiao et al. 2022), and lotion polymerization method (Wang et al. 2022b). The solvothermal method can directly produce hollow spheres on its surface through adsorption or chemical reactions using surfactants as templates, which has been proven to be a convenient and effective synthesis strategy (Wu et al. 2021).

In this study, a series of mesoporous $NaAlSiO_4$ hollow microspheres were synthesized through the solvothermal method combined with high-temperature calcination. The physicochemical properties of the as-synthesized mesoporous $NaAlSiO_4$ hollow microspheres were characterized through elemental analysis, FTIR, SEM, TEM, XRD and TG-DSC. The adsorption performance of mesoporous $NaAlSiO_4$ hollow microspheres was evaluated using Ni(II) and Cd(II) as the models under different adsorption conditions, such as initial pH, concentration of different ions and adsorption time. Accordingly, the adsorption mechanism of heavy metal ions by mesoporous $NaAlSiO_4$ hollow microspheres was analyzed and discussed. There are few studies on the use of $NaAlSiO_4$ microspheres as adsorbents to adsorb heavy metal ions. Thus, this study provides an effective absorbent for removing heavy metal ions in wastewater treatment and environmental remediation.

2 Materials and Methods

2.1 Materials

Chemical reagents, including tetraethyl orthosilicate (TEOS), sodium aluminate, hexadecyl trimethyl ammonium bromide (CTAB), sodium hydroxide (NaOH), hydrochloric acid (HCl), nickel acetate tetrahydrate (Ni(II)), cadmium sulfate, 8/3-hydrate (Cd(II)), ammonia solution, and absolute ethanol, were purchased from Sinopharm Chemical Reagent Co., Ltd. (Shanghai, China). All reagents and solutions were reagent grade.

2.2 Synthesis of Mesoporous $NaAlSiO_4$ Hollow Microspheres

In a typical synthesis, two precursor solutions were prepared. TEOS and CTAB were dissolved in 30 mL of ethanol to obtain solution (A) Sodium aluminate was then dissolved in 40 mL of deionized water to obtain solution (B) Afterwards, solution B and 10.8 mL ammonia solution (10 mL of deionized water and 0.8 mL of ammonia solution) were dripped into solution A to form a homogeneous suspension. The mixed solution was transferred into a 100 mL Teflon autoclave and heated at designed temperatures for different times in a vacuum dryer. After hydrothermal treatment, the product was centrifuged, washed three times with deionized water and ethanol, and then dried at 60 °C for 24 h. The resulting product was calcined in a muffle furnace to remove the CTAB in the microspheres.

2.3 Characterizations

The crystal structure of the samples was characterized by X-ray diffraction (XRD) (D8-ADVANCE, Germany) with Cu Kα radiation (λ = 1.5406 Å). Transmission electron microscopy (TEM) and high-resolution TEM (HRTEM) images were collected using a field emission high-resolution transmission electron microscope (JEM-2100 F, Japan) at a 200 kV operating voltage. FT-IR spectra of the mesoporous $NaAlSiO_4$ hollow microspheres were obtained on a nexus spectrometer (Nexus, America) using a Nd YVO_4 laser (1064 nm). DSC-DTA was measured by Diamond TG/DTA (Perkin Elmer, America). Microscopic photographs of the mesoporous $NaAlSiO_4$ hollow microspheres were taken using a scanning electron microscope (SEM) (JEM-2100 F, Japan). The specific surface area and pore size of

the microspheres were measured by an automatic surface area and porosity analyzer (ASAP 2460). The determination of ion concentrations was tested by an atomic absorption spectrometer (CONTRAA-700, German). The zeta potential of the samples was measured using a zeta potential analyzer (Nano ZS ZEN3600) at room temperature.

2.4 Adsorption Properties of Mesoporous $NaAlSiO_4$ Hollow Microspheres

The adsorption properties of mesoporous $NaAlSiO_4$ hollow microspheres were evaluated using Ni(II) and Cd(II) as models. In a typical experiment, the sample (20 mg) was added to 10 mL of ionic solution (cadmium sulfate, 200 mg/L; nickel acetate, 200 mg/L). All adsorption experiments were conducted at 25 ± 0.5 °C and stirred at an agitation rate of 100 rpm. The supernatant was collected at designated time intervals. The adsorption performance of different samples was assessed by monitoring the change in ion concentrations.

The amounts of metallic ions adsorbed per unit mass of the adsorbent were determined using the following equation:

$$q_e = \frac{C_0 - C_e}{m} V \tag{1}$$

$$RE\,(\%) = \frac{C_0 - C_e}{C_0} 100\% \tag{2}$$

where q_e is the amount adsorbed per unit mass of the adsorbent (mg/g), C_0 and Ce are the initial and equilibrium concentrations of the adsorbate, respectively (mg/L), m is the mass of adsorbent (g), V (L) is the volume of the solution, and RE (%) is the ion adsorption rate of Ni(II) and Cd(II).

2.5 Regeneration and Reusability

For the regeneration and reusability study, the spent adsorbent was gently washed with deionized water, followed by immersion in 20 mL of 0.01 NaOH for 3 h. The adsorbents were then collected and cleaned with deionized water until neutral conditions. The consecutive adsorption/desorption cycles were repeated three times.

3 Results and Discussion

3.1 Synthesis Mechanism of Mesoporous $NaAlSiO_4$ Hollow Microspheres

Mesoporous $NaAlSiO_4$ hollow microspheres were synthesized through a solvothermal method. In a typical synthesis, an ethanol-water mixture containing CTAB was employed to stabilize the oil droplets of TEOS to form micelles and serve as the templates for the formation of mesoporous $NaAlSiO_4$ hollow microspheres. When ammonia aqueous solution was added into the system, TEOS on the interface was hydrolyzed, and silica was deposited on the interface. Since the concentration of TEOS decreased on the interface, the concentration difference of TEOS in the oil droplets diffused from the inside to the interface (Liang et al.

2020). At the same time, sodium aluminate was involved in the hydrolysis of TEOS to form $NaAlSiO_4$ under the conditions of high temperature and pressure. Thus, $NaAlSiO_4$ hollow microspheres can be achieved after calcination (Fig. 1). The CTAB surfactant directs the formation of meso-structures of mesoporous $NaAlSiO_4$ hollow microspheres. If too little ethanol is introduced into the system, the hydrolysis of TEOS is so fast that near the surface of the droplets, the ethanol concentration is much higher, and the TEOS inside the oil droplets cannot diffuse so fast outwards. However, if the ethanol in the system is redundant, the suppressing effect of ethanol makes the TEOS near the surface of the droplets remain the same, and the inner TEOS cannot diffuse outwards; after calcination, the spheres become solid (Wang et al. 2021). Therefore, the resultant products are not hollow microspheres. By adjusting the ratio of ethanol and water in the experiment, the ratio that can form hollow microspheres is finally determined to be 0.6. Therefore, this experiment was carried out with an ethanol to water ratio of 0.6.

3.2 Characteristics of Mesoporous $NaAlSiO_4$ Hollow Microspheres

The influences of synthesis parameters, such as the reaction temperature, the reaction time, and the molar ratio of reactants, have been investigated in detail. Figure 2A and C show SEM images of the samples synthesized at different TEOS/sodium aluminate mole ratios (Si/Al mole ratio). When the Si/Al ratio was 2:1, the microspheres shown in Fig. 2A were

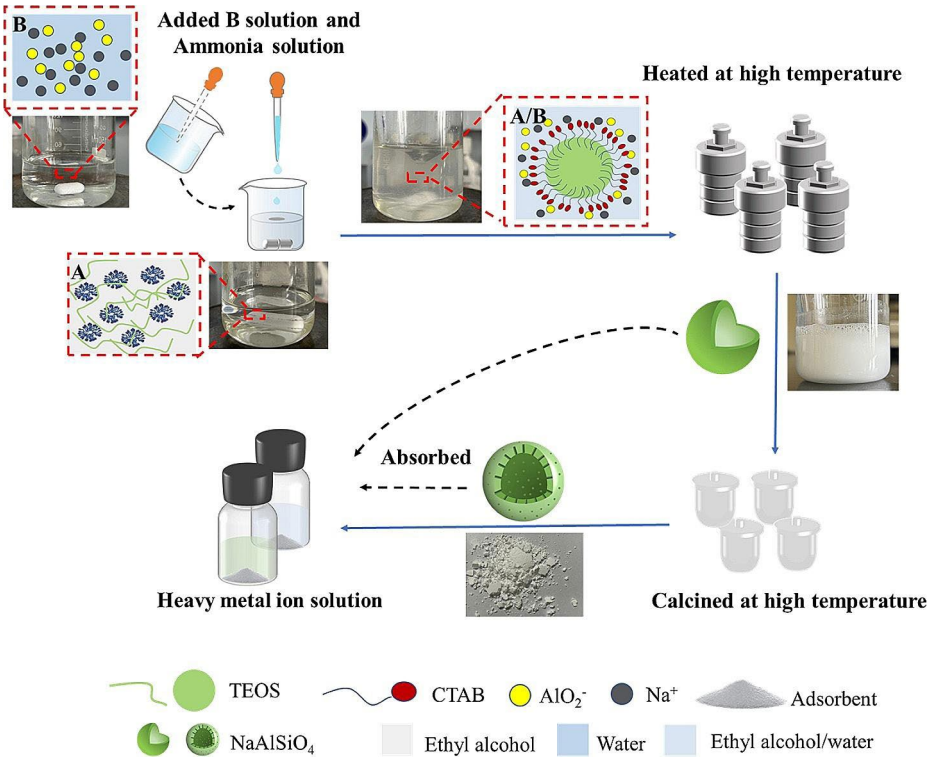

Fig. 1 Synthesis and heavy metal ion adsorption of the hollow $NaAlSiO_4$ microspheres

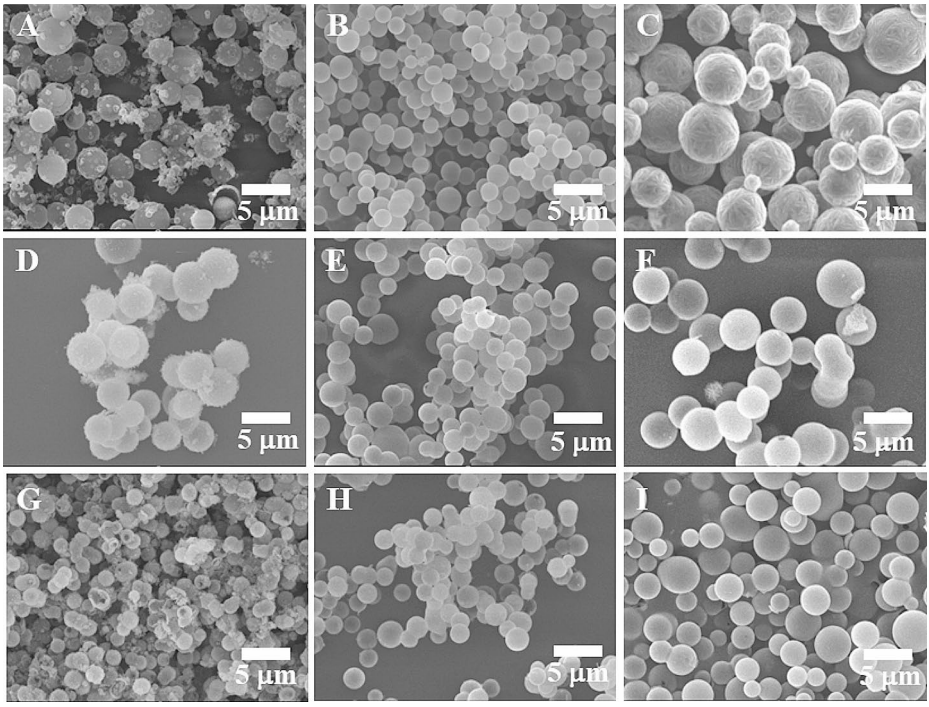

Fig. 2 SEM image of mesoporous $NaAlSiO_4$ hollow microspheres under different conditions. (**A-C**) Si/Al mole ratios of 2:1, 1:1, and 1:2, respectively; (**D-F**) CTAB concentrations of 0.02 mol/L, 0.04 mol/L, and 0.06 mol/L, respectively; (**G-I**) reaction times of 3 h, 18 h, and 36 h, respectively

seriously broken, and it was difficult to form a uniform microsphere. This is because the high concentration of TEOS makes it easy for the reaction system to form gels, resulting in rapid solidification and crack formation on the surface of the microspheres. However, when the Si/Al ratio was 1:2, the microspheres in Fig. 2C show an increase in apparent roughness and a large size distribution. By comparison, microspheres of uniform size were obtained, as shown in Fig. 2B, when the Si/Al ratio was 1:1. Numerous studies have shown that specific surfactants can interact with inorganic substances to form different surface structures (Liu et al. 2020). Figure 2D and F show the effect of different CTAB concentrations on the morphology of the microspheres. When the concentration of CTAB was 0.02 mol/L, the obtained microspheres had an irregular spherical shape due to the low concentration of template molecules. When the concentration of CTAB was 0.04 mol/L, a regular and relatively uniform spherical shape was formed. When the concentration of CTAB was increased to 0.06 mol/L, larger microspheres were obtained due to the excessive CTAB. Figure 2G and I show the effect of the reaction time from 3 h to 18 h on the morphology of the microspheres. The microspheres were incompletely assembled when the reaction time was 3 h (Fig. 2G). The microspheres completely assembled at a uniform size when extending the reaction time to 18 h (Fig. 2H). The particle size of the microspheres was not uniformly distributed when the reaction was carried out for more than 18 h (Fig. 2I). Therefore, the optimal conditions for forming mesoporous hollow microspheres are as follows: Si/Al ratio of 1:1, CTAB con-

centration of 0.04 mol/L, reaction temperature of 150 °C, and reaction time of 18 h. The average diameter of the as-synthesized microspheres is approximately 2 ± 0.5 μm.

The DSC-TG curves of the as-synthesized microspheres were recorded up to 1400 °C, as shown in Fig. 3A. Two mass loss processes are observed in the TG curve. The first mass loss of approximately 10 wt% occurring in the temperature range of 25~200 °C could be ascribed to the removal of physically adsorbed water, while the second mass loss of approximately 7.4 wt% ranging from 200 to 550 °C could be ascribed to the removal of crystal water and degradation of CTAB. The peak near 301 °C in the DSC curve indicates the endothermal process derived from the removal of the crystal water and degradation of CTAB, the peak near 707 °C indicates the crystal transformation from an amorphous state to a well-crystallized state.

The XRD analysis of the microspheres is shown in Fig. 3B. The crystal diffraction peaks appeared after the microspheres were calcined at 850 °C. The diffraction peaks near 21.2°, 24.5°, 29.3°, 35.0°, and 41.4° can be indexed to the (111), (121), (211), (141), and (151) crystal planes, respectively, of $NaAlSiO_4$ (standard card PDF No. 52-1342). The results above prove that the synthesized microspheres are $NaAlSiO_4$ microspheres. No obvious diffraction peaks were observed in the XRD patterns of the microspheres before and after calcination at temperatures lower than 750 °C, implying that amorphous $NaAlSiO_4$ microspheres were formed below 750 °C. Compared with the microspheres without calcination, the diffraction peaks of the microspheres calcined at 750 °C and 550 °C shifted to a smaller

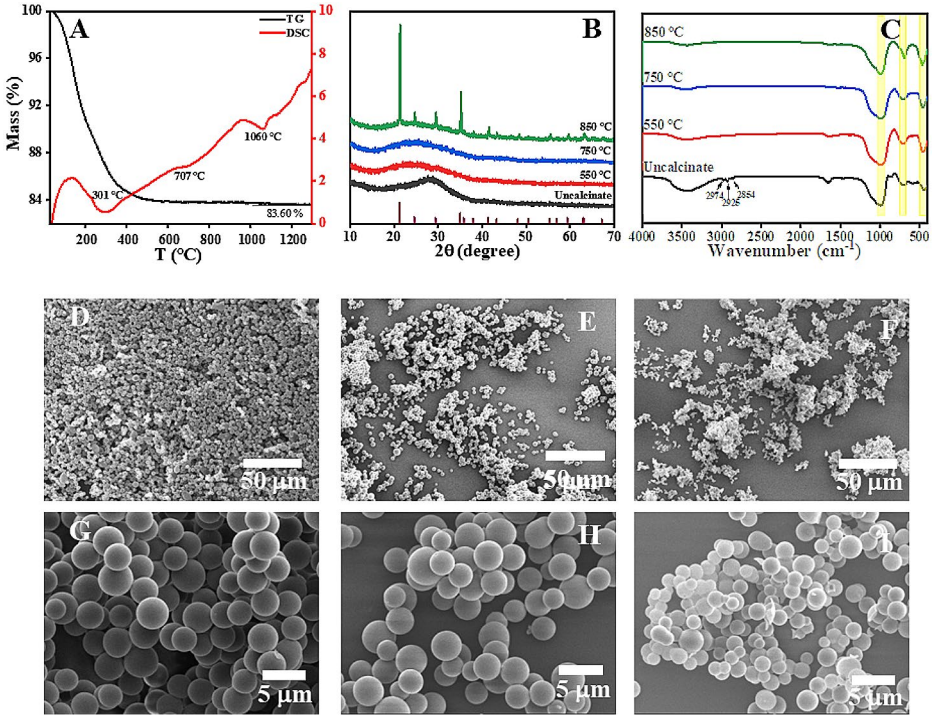

Fig. 3 Influence on the structure and morphology of the $NaAlSiO_4$ microspheres before and after calcination at different temperatures. (**A**) TG-DSC curve; (**B**) XRD patterns; (**C**) FT-IR spectra; SEM images of the $NaAlSiO_4$ microspheres calcined at 550 °C (**D**, **G**), 750 °C (**E**, **H**), and 850 °C (**F**, **I**)

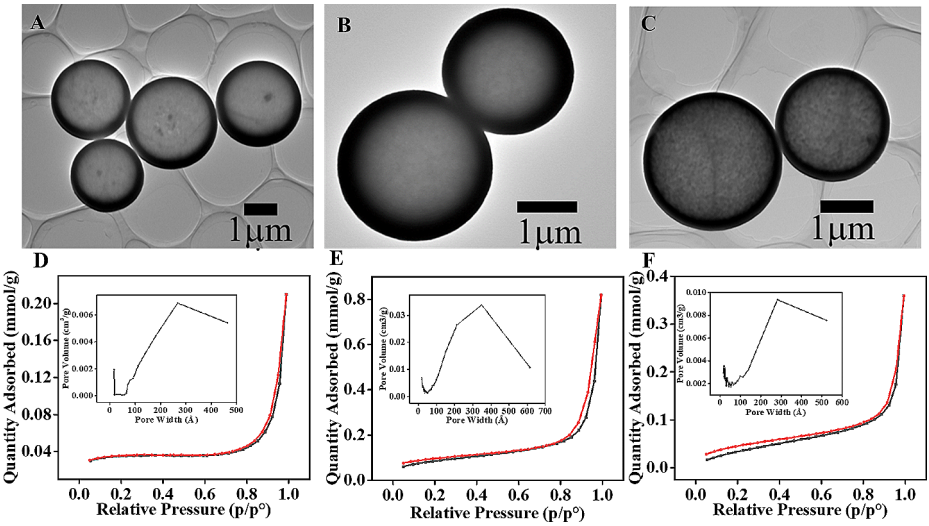

Fig. 4 The internal structure of the $NaAlSiO_4$ microspheres before and after calcination at different temperatures. (**A**)-(**C**) TEM images of the hollow microspheres before and after calcination at 550 °C and 750 °C, respectively. (**D**)-(**F**) N_2 adsorption-desorption isotherms and pore size distribution of the hollow microspheres before and after calcination at 550 °C and 750 °C, respectively

angle with lager peak width, suggesting that the crystal plane spacing of the microspheres becomes larger and the grain size becomes smaller. These results indicate that well-crystallized $NaAlSiO_4$ microspheres can be obtained after calcination at 850 °C.

The surface information of the $NaAlSiO_4$ microspheres was analyzed through FT-IR spectra. Figure 3C shows FT-IR spectra of the microspheres before and after calcination at different temperatures. Three peaks, near 2854 cm^{-1}, 2925 cm^{-1}, and 2974 cm^{-1}, corresponding to the asymmetric and symmetric CH_2 stretching modes of the amine groups of CTAB in the microspheres disappeared after calcination at temperatures above 550 °C, indicating that CTAB was almost completely degraded when the calcination temperature was above 550 °C. The peak near 443 cm^{-1} is due to the Si-O or Al-O bending mode, the peak near 714 cm^{-1} is ascribed to the symmetric stretch vibration of the internal tetrahedron, and the peak near 1000 cm^{-1} is due to the anti-symmetric stretching vibration of Si-O-Si. These results agree well with those of the XRD characterization. The morphologies of the microspheres after calcination are shown in Fig. 3D and I. The results show that the $NaAlSiO_4$ microspheres retain an integral and smooth spherical shape without obvious changes in size distribution after calcinating at 550 °C (Fig. 3D and G) and 750 °C (Fig. 3E and H), while slight aggregations of the microspheres were observed when calcinating at 850 °C (Fig. 3F and I).

The internal structure of the $NaAlSiO_4$ microspheres was characterized through TEM observation and N_2 adsorption-desorption measurements (Fig. 4). TEM images show the hollow internal structure of the $NaAlSiO_4$ microspheres before and after calcination at 550 °C and 750 °C. No obvious change in the morphology and internal structure of the hollow microspheres was observed after calcination (Fig. 4A and C). Figure 4D and F show the N_2 adsorption-desorption isotherms of the $NaAlSiO_4$ hollow microspheres before and after calcination at different temperatures. The N_2 adsorption-desorption isotherms of the hollow

microspheres were indexed to type IV. The isotherm of the $NaAlSiO_4$ hollow microspheres before calcination displays a hysteresis loop at a relative pressure (p/p_0) of 0.8-1.0, indicating the formation of mesopores and macropores. The shape of the hysteresis loop is of type H1, implying the formation of ordered mesopores in the shell of the hollow microspheres. However, when calcined at 550 °C and 750 °C, the N_2 adsorption-desorption isotherm of the hollow microspheres remains unclosed in a wide range of p/p_0 from 0.1 to 1.0, which can be attributed to the irreversible adsorption-desorption process of N_2 because of the presence of micropores (Wu et al. 2022). The analysis of the pore size distribution of the $NaAlSiO_4$ hollow microspheres shows that two remarkable peaks appear at approximately 20 nm and 35 nm when calcinating the microspheres at 550 °C, while only one peak appears at approximately 27 nm before and after calcinating the microspheres at 750 °C. Meanwhile, the specific surface area calculated from the N_2 adsorption isotherm according to the BET method was approximately 3.5 m^2/g, 15.1 m^2/g, and 10.5 m^2/g for the $NaAlSiO_4$ hollow microspheres before and after calcination at 550 °C and 750 °C, respectively. It is speculated that the grain growth in the shell of the $NaAlSiO_4$ hollow microspheres squeezes the space of micropores, and thus, results in a decrease in the pore size and specific surface area when calcinated at a higher temperature (750 °C). These results demonstrate that calcination treatment plays a crucial role in the pore formation and pore size of the $NaAlSiO_4$ hollow microspheres.

3.3 Adsorption Properties of Mesoporous $NaAlSiO_4$ Hollow Microspheres

Removal of heavy metal ions by the $NaAlSiO_4$ hollow microspheres was evaluated using Ni(II) and Cd(II) as the models under different conditions. As shown in Fig. 5A and E, the adsorption capacity of the hollow microspheres for both Ni(II) and Cd(II) increases sharply in the initial stage (2 h) and then reaches equilibrium. We can divide the adsorption process into two periods. The first period includes rapid adsorption of ions on the outer surface of adsorbents; once the exterior surface of the adsorbent is fully saturated, the second period of adsorption starts. In the second period, adsorption is performed via the diffusion of ions into the inner surface of the adsorbent (Yuan et al. 2022). It is very interesting that the $NaAlSiO_4$ hollow microspheres after calcination at 550 °C displayed the highest adsorption capacity for Ni(II), and the hollow microspheres without calcination displayed the highest adsorption capacity for Cd(II). At the same dose of hollow microspheres (0.02 g), the adsorption capacity of heavy metal ions significantly increased as the initial concentration of heavy metal ions increased. The adsorption of Cd(II) by the hollow microspheres without calcination reached saturation at a concentration of approximately 106.03 ± 0.97 mg/g, while the adsorption of Ni(II) by the hollow microspheres after calcination at 550 °C did not reach saturation at a concentration of more than 115.15 ± 1.68 mg/g (Fig. 5B and F). The adsorption capacity of Ni(II) and Cd(II) by $NaAlSiO_4$ microspheres is better than that of the adsorbents reported in most studies (Table 1). To further evaluate the removal capacity of the hollow microspheres, different doses from 0.01 g to 0.2 g of hollow microspheres were used without changing the concentrations of Ni(II) and Cd(II). The results show that the removal efficiency for Ni(II) increased from approximately 60–90% when the dose of the hollow microspheres after calcination at 550 °C changed from 0.01 g to 0.2 g, while the removal efficiency for Cd(II) reached approximately 99% by the hollow microspheres without calcination at a dose of 0.05 g. These results indicate a higher removal capacity for

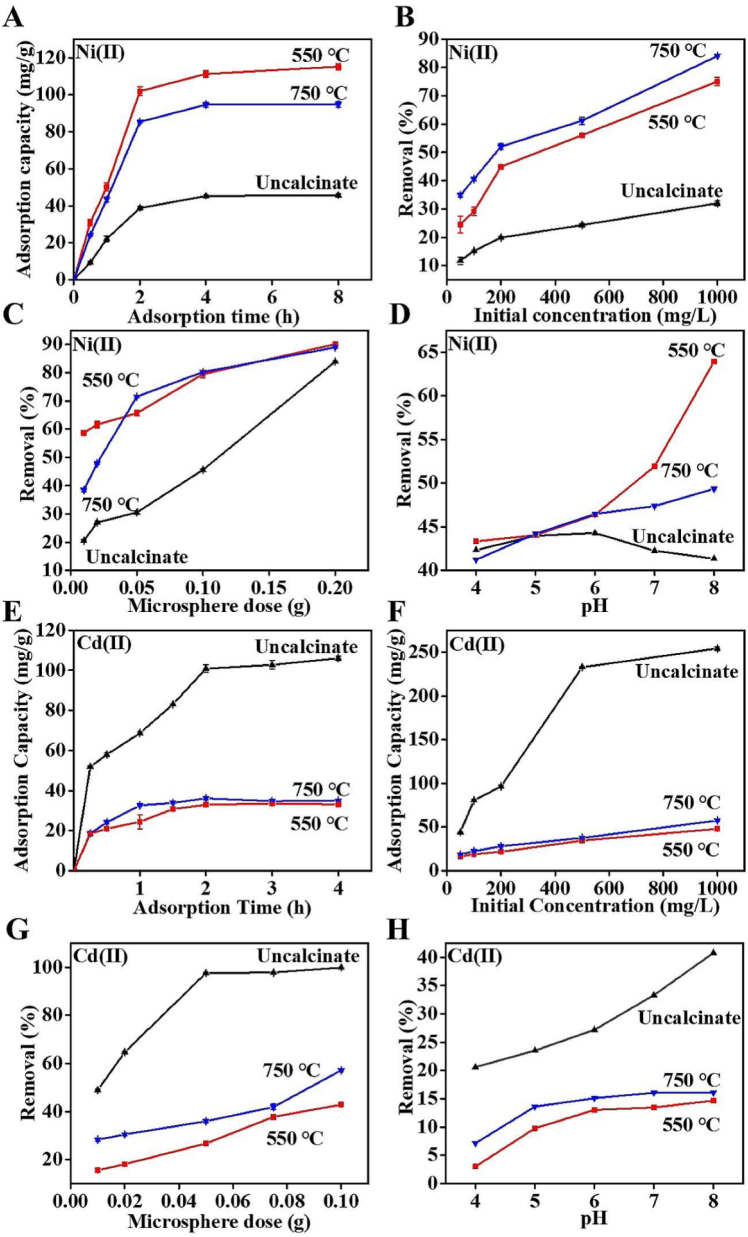

Fig. 5 Removal of heavy metal ions (Ni(II) and Cd(II)) by the $NaAlSiO_4$ hollow microspheres under different conditions. (**A-D**) Removal of Ni(II) by the microspheres under different conditions. (**E-H**) Removal of Cd(II) by the hollow microspheres under different conditions

Table 1 Comparison of the maximum adsorption capacity with different materials reported in the literature for Ni(II) and cd(II)

Used materials	Ni(II) (mg/g)	Ref.	Used materials	Cd(ll) (mg/g)	Ref.
Graphene oxide (GO)	20.19	(Salihi et al. 2016)	Mesoporous carbon stabilized alumina	49.98	(Yang et al. 2016)
Sodium dodecyl suphate modified graphene oxide (GO)	55.16	(Salihi et al. 2016)	Hierarchical vaterite spherulites	984.5	(Chen et al. 2018)
Manganese dioxide	114.9	(Ong et al. 2018)	Fe_3O_4@mesoporousSiO_2	51.81	(Tang et al. 2013)
Activated alumina	71.43	(Rajurkar et al. 2011)	Al_2O_3	88.26	(Liu et al. 2022)
Hydrous TiO_2	22.7	(Debnath and Ghosh 2009)	MgO nanoparticles	2294	(Xiong et al. 2015)
Lignocellulose/montmorillonite nanocomposite	94.86	(Zhang and Wang 2015)	Mesoporous activated carbon	27.3	(Boumediene et al. 2015)
Nigerian kaolinite clay	167	(Dawodu and Akpomie 2014)	Graphene oxide/polyamidoamine dendrimers	253.81	(Zhang et al. 2014)
Nigerian kaolinite clay	65	(Malayoglu 2018)	nanofibers	148.79	(Karim et al. 2019)
UThis work	297.11		This work	449.71	

Ni(II) by the $NaAlSiO_4$ hollow microspheres after calcination at 550 °C and for Cd(II) by the hollow microspheres without calcination (Fig. 5C and G).

It is well known that the pH value of the solution affects the adsorption-association process of metal ions on the surface of the absorbents. Therefore, the pH value of the suspension was adjusted from 4.0 to 8.0 to evaluate the effect of different pH values on the adsorption capacity of the hollow microspheres (Fig. 5D and H). The results show that the removal efficiency of both Ni(II) and Cd(II) by the hollow microspheres was greatly decreased under acidic conditions (pH = 4.0) and significantly increased under alkaline conditions (pH = 8.0).

The adsorption capacities increased with increasing concentration of heavy metal ions and gradually achieved a maximum adsorption value, which is noted as the maximum adsorption captivity. It is obvious that the ratio of available binding sites to the total metal ions was higher at low concentrations than that at high concentration. All metal ions could be bound to the active sites of the microspheres in this case. Therefore, the binding was dependent on the initial concentration (Guo et al. 2022a). Equilibrium was also reached after an adsorption time exceeding 2 h. Na(I) affects the adsorption of Ni(II), so the adsorption mechanism of the adsorbent for Ni(II) can only rely on the mesoporous adsorption mechanism. However, Na(I) has little effect on the adsorption of Cd(II), so the adsorption mechanism of the adsorbent for Cd(II) is electrostatic adsorption, which mainly depends on the CTAB contained in the microspheres (Awual et al. 2014). When adsorbing Ni(II), the microspheres calcined at 550 °C have the best adsorption effect because they have the highest specific surface area. However, when adsorbing Cd(II), due to the polar part of CTAB having a main adsorption capacity for Cd(II), the microspheres uncalcined with CTAB have the best adsorption effect. Therefore, the microspheres without calcination treatment prefer to adsorb Cd(II). With increasing adsorbent content, the adsorption efficiency was obviously improved. This is because a higher adsorption dose provides more chelating active sites to

be exposed in solution, and metal ions can have more opportunities to bind with free active groups.

The different pH of the solution resulted in the difference of the adsorption capacity of the microspheres. At low pH values, various functional groups in the microspheres were protonated, and thus, electrostatic repulsion occurred between the microsphere chains and the metal ions, leading to poor bonding. As the pH of the solution increased, the electrostatic repulsion between the mesoporous $NaAlSiO_4$ hollow microspheres and the metal ions weakened. Thus, the metal ions could easily access chelating active sites, which resulted in high removal efficiency (Xu et al. 2017). Therefore, the increase in pH enhances the electrostatic attraction between the adsorbent and Cd(II). In Fig. 6A, when the pH of the solution was adjusted to 8.0, there is obvious precipitation in the solution with the increase of the concentration of Cd(II). At the same pH value, when the concentration of Ni(II) is 500 mg/L and 1000 mg/L, the precipitation was also observed. When Ni(II) is in basic condition, Ni(II) reacts with hydroxide ions to form hydroxylated complexes, which may be due to the combination of both adsorption and precipitation on the surface of microsphere-metal ion nanoparticles (Adham Ahmed 2010; Cai et al. 2020). Therefore, the increase in

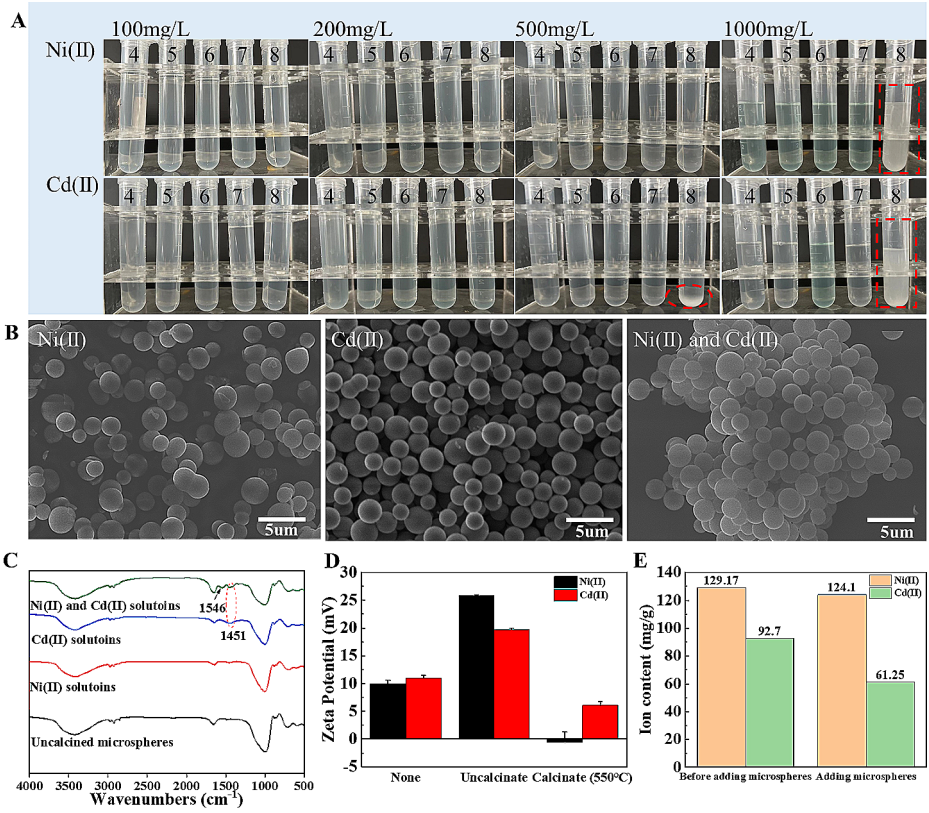

Fig. 6 The $NaAlSiO_4$ hollow microspheres with adsorbed ions. (**A**) Photos of Ni(II) and Cd(II) state in different pH (regulated pH with HCl, 0.005 mol/L, and NaOH, 0.01 mol/L), (**B**) SEM images, (**C**) FT-IR spectra, (**D**) The corresponding zeta potential before and after adsorption of ions by microspheres at pH = 7. (**E**) Ion competitive adsorption of Ni(II) and Cd(II) by the $NaAlSiO_4$ hollow microspheres. The Ni(II) and Cd(II) concentrations are 100 mg/L

pH also significantly enhances the electrostatic attraction between the adsorbent calcined at 550 °C and Ni(II). When the pH of the solution was 8.0, the ions in the solution are precipitated, resulting in a sharp increase in the adsorption capacity of the microspheres. No precipitation occurs in lower ion concentrations or lower pH solutions. SEM images show that no obvious precipitate was found on the surface of the microspheres (Fig. 6B). FT-IR spectra (Fig. 6C) show obvious changes of chemical bond in the case of the Cd(II) adsorption by uncalcinated microspheres. There are no obvious chemical bond changes from other groups, implying that the adsorption of Cd(II) by the microspheres was mesoporous adsorption and chemical adsorption, and the adsorption of Ni(II) was mainly mesoporous adsorption. According to the comparison of the surface charge (Fig. 6D), the obvious changes of Zeta potential for the microspheres before and after the Cd(II) and Ni(II) adsorption were observed. These results verify that the microspheres have different adsorption mechanisms for different ions. Under the optimal conditions for adsorption and the Ni(II)/Cd(II) ratio of 1:1, the adsorption capacity of the uncalcined microspheres for Cd(II) is stronger than that of Ni(II) (Fig. 6E), which also validates the above inference on the adsorption performance.

In order to explore the adsorption mechanism of the $NaAlSiO_4$ hollow microspheres, the experimental data were fitted into different kinetic models, including pseudo-first-order, pseudo-second-order, Langmuir, and Freundlich models.

The pseudo-first-order model is formulated as:

$$\ln (q_e - q_t) = \ln q_e - k_1 t \tag{3}$$

The pseudo-second-order equation based on adsorption equilibrium capacity is represented by:

$$\frac{t}{q_t} = \frac{1}{k_2 q_e^2} + \frac{1}{q_e} t \tag{4}$$

where q_e and q_t (mg/g) are the amounts of Ni(II) or Cd(II) ions adsorbed at equilibrium and time t (min), respectively; k_1 and k_2 are the equilibrium rate constants of the pseudo-first-order adsorption (min^{-1}) and the pseudo-second-order adsorption (g mg^{-1} min^{-1}), respectively. The plot of $\ln(q_e\text{-}q_t)$ versus t gives the k_1 and q_e values. k_2 and q_e (mg/g) can be obtained from the intercept and slope of the plot of (t/q_t) versus t (min). The kinetic parameters and the linear plots of the pseudo-first-order and the pseudo-second-order kinetic model of Ni(II) and Cd(II) adsorption on the $NaAlSiO_4$ hollow microspheres are shown in Fig. 7A and B, and 7E and 7F. In this study, the adsorption amounts at different adsorption times were measured at a Ni(II) and Cd(II) concentration of 100 mg/L with the pH of 7.0 at 25 °C. Further, the calculated q_e values for Ni(II) or Cd(II) were 143.08 mg/g and 115.71 mg/g, respectively, according to pseudo-second-order model. The correlation coefficient (R^2) and constant are determined by the equation (as shown in Fig. 7A, B and E, and 7F). As it can be seen from Table 2, the adsorption curves of Ni(II) (adsorbent calcined at 550 °C) and Cd(II) (adsorbent without calcination) show that the removal process accords with the pseudo-second-order model with good linearity (R^2=0.92 and 0.97). Therefore, the pseudo-second-order kinetic equation is more suitable to describe the adsorption of Ni(II) and Cd(II) on the $NaAlSiO_4$ hollow microspheres, mainly due to the interaction between metal ions and microspheres such as ion exchange and surface combination.

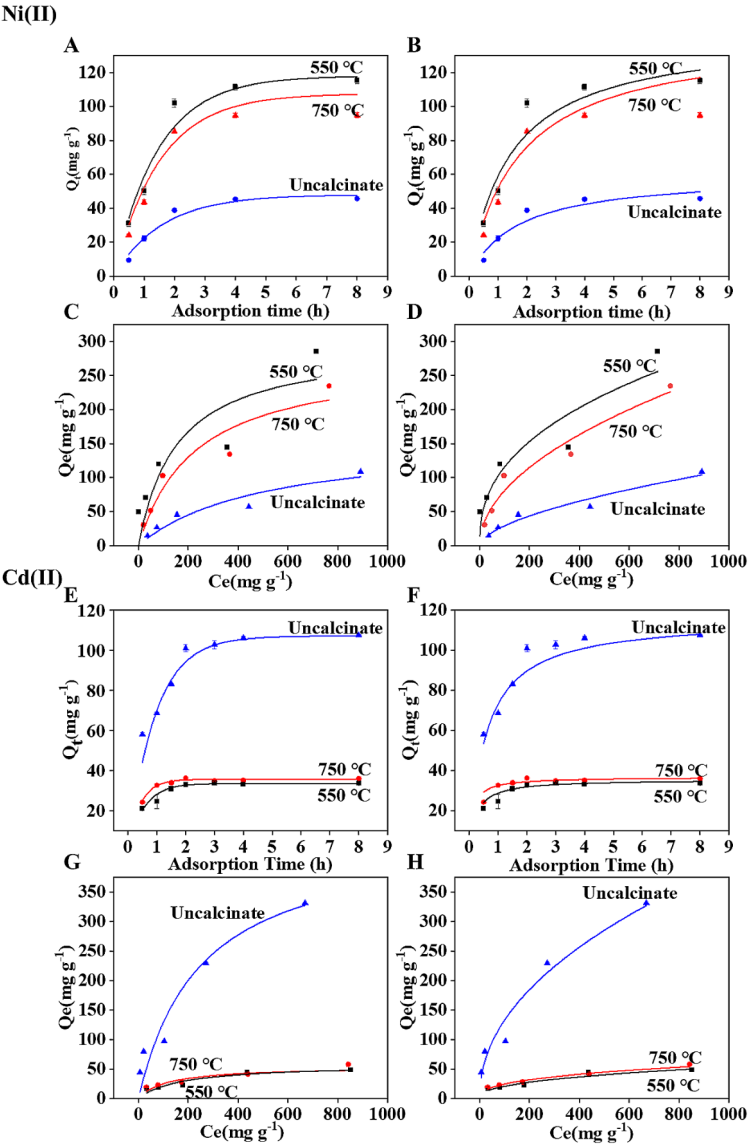

Fig. 7 The first-order, pseudo-second-order, Langmuir and Freundlich models of Ni(II) (**A-D**) and Cd(II) adsorption (**E-H**)

The adsorption isotherms of Ni(II) and Cd(II) by the hollow microspheres were also fitted according to Langmuir and Freundlich equation.

The Langmuir equation is formulated as:

$$\frac{C_e}{q_e} = \frac{1}{K_L q_{max}} + \frac{C_e}{q_{max}} \tag{5}$$

Table 2 Fitting parameter calculated from pseudo-first-order and pseudo-second-order models

		pseudo-first-order			pseudo-second-order		
		q_e (mg/g)	k_1 (min^{-1})	R^2	q_e (mg/g)	k_2 ($g.mg^{-1}.min^{-1}$)	R^2
Ni(II)	Uncalcinated	47.98	624×10^{-3}	0.96	60.09	4.04×10^{-3}	0.88
	550 °C	118.05	686×10^{-3}	0.96	143.08	4.91×10^{-3}	0.92
	750 °C	107.60	661×10^{-3}	0.94	142.41	9.87×10^{-3}	0.92
Cd(II))	Uncalcinated	106.98	1061×10^{-3}	0.94	115.71	14.81×10^{-3}	0.97
	550 °C	33.50	1826×10^{-3}	0.96	35.55	117.66×10^{-3}	0.78
	750 °C	35.52	2429×10^{-3}	0.90	36.54	216.66×10^{-3}	0.87

Table 3 Fitting parameter calculated from Langmuir and Freundlich models

		Langmuir			Freundlich		
		q_{emax} (mg/g)	K_L ($L.mg^{-1}$)	R^2	K_F ($mg^{1-n}\cdot L^n.g^{-1}$)	n	R^2
Ni(II)	Uncalcinate	157.01	2.02×10^{-3}	0.91	2.01	580.52×10^{-3}	0.96
	550°C	297.11	6.49×10^{-3}	0.74	18.07	2478×10^{-3}	0.86
	750°C	277.49	4.42×10^{-3}	0.91	7.94	504.5×10^{-3}	0.96
Cd(II))	Uncalcinate	449.71	4.02×10^{-3}	0.92	14.98	2110×10^{-3}	0.98
	550°C	57.38	5.67×10^{-3}	0.89	3.08	2426×10^{-3}	0.94
	750°C	53.77	8.5×10^{-3}	0.73	4.28	2657×10^{-3}	0.95

The Freundlich equation is formulated as:

$$\ln q_e = \ln K_F + \frac{1}{n}\ln C_e \tag{6}$$

where q_{max} (mg/g) is the maximal adsorption capacity, q_e (mg/g) and c_e (mg/L) are the equilibrium adsorption capacity and equilibrium concentration of Ni(II) or Cd(II) ions, respectively. n is the parameter of Freundlich adsorption isotherm. K_L ($L\cdot mg^{-1}$) and K_F ($mg^{1-n}.L^n.g^{-1}$) are the equilibrium constants of the Langmuir and Freundlich equations, respectively. The fitting of adsorption data is shown in Fig. 7C, D and G, and 7H. Table 3 summarizes the Langmuir and Freundlich model constants calculated by the equation. In terms of relevant parameters, the Ni(II) adsorption data fitted by the Freundlich model (adsorbent calcined at 550 °C) is superior to the Ni(II) adsorption data fitted by the Langmuir isothermal model. According to the Langmuir fitting model, the maximum adsorption capacity of $NaAlSiO_4$ microspheres for Ni(II) is 297.11 mg/g. Combined with the structural characterization of the obtained samples, the porous structure of the prepared microspheres is mainly responsible for Ni(II) removal. The Cd(II) adsorption data fitted by Langmuir model is better than that fitted by Freundlich isothermal model, indicating that the removal of Cd(II) on microsphere is monolayer adsorption. The electrostatic interaction and formation of complex on the surface of microsphere are the main mechanism of Cd(II) adsorption by the $NaAlSiO_4$ microspheres. According to the Langmuir fitting model, the maximum adsorption capacity of the $NaAlSiO_4$ microspheres for Cd(II) is 449.71 mg/g.

3.4 Regeneration and Reusability of Mesoporous $NaAlSiO_4$ Hollow Microspheres

The recycling of the hollow $NaAlSiO_4$ microspheres adsorbing heavy metal ions was evaluated by immersing the saturated hollow microspheres in a NaOH solution (0.01 mol/L). As shown in Fig. 8A and B, almost no obvious decrease in the Ni(II) adsorption efficiency of the $NaAlSiO_4$ hollow microspheres was observed after desorption treatment. The adsorption efficiency remained above 95% of the original efficiency after three repeated experiments. In contrast, the adsorption efficiency for Cd(II) by the hollow microspheres was significantly decreased even after one desorption treatment. It is speculated that when the microsphere adsorbs Cd(II) for the first time, Cd(II) and CTAB form a complex, and the ions cannot be effectively released during the desorption process, so the efficiency of multiple adsorption is reduced (Awual et al. 2014; Yun-Kai Lu 2004).

4 Conclusions

In summary, a novel strategy has been developed to synthesize a series of $NaAlSiO_4$ hollow microspheres for Ni(II) and Cd(II) removal from wastewater by combining a hydrothermal method with calcination treatment. The average diameter of the hollow microspheres is approximately 2 ± 0.5 μm. The specific surface area and pore size are approximately 3.5 m^2/g and 27 nm for the hollow microspheres without calcination, 15.1 m^2/g and 20 ~ 35 nm, and 10.5 m^2/g and 27 nm for the hollow microspheres after calcination at 550 °C and 750 °C, respectively. The adsorption mechanism of the $NaAlSiO_4$ adsorbent for Ni(II) relies on the mesoporous adsorption mechanism. The adsorption mechanism of the adsorbent for Cd(II) is electrostatic adsorption, which mainly depends on the CTAB contained in the microspheres. The $NaAlSiO_4$ hollow microspheres display a high adsorption capacity for different heavy metal ions after the calcination treatment. The results show that the hollow $NaAlSiO_4$ microspheres without calcination prefer to remove Cd(II) at a maximum adsorption capacity of 449.71 mg/g, while the hollow microspheres after calcination at 550 °C are beneficial for removing Ni(II) at a maximum adsorption capacity of 297.11 mg/g calculated from Langmuir models. Not only can the adsorption capacity of Ni(II) and Cd(II) be changed

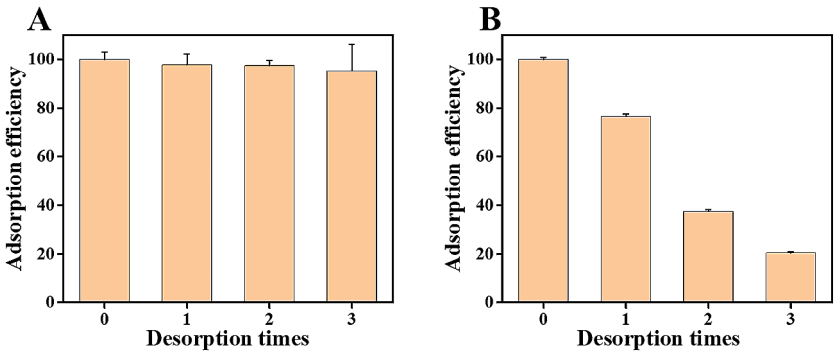

Fig. 8 The recycling of the hollow $NaAlSiO_4$ microspheres after desorption treatment using NaOH solution. **(A)** Ni(II), **(B)** Cd(II)

by calcination, but also the $NaAlSiO_4$ hollow microspheres after calcination at 550 °C was regenerated with NaOH solution treatment and able to be reused in many cycles without significant deterioration in its subsequent performances. These results provide a novel and facile strategy to synthesize $NaAlSiO_4$ hollow microspheres as adsorbents for the removal of heavy metal ions in wastewater treatment and other environmental remediation.

Acknowledgements This work was financially supported by the National Key Research and Development (R&D) Program of China (No. 2018YFB1105702).

Author Contributions Z.O. and L.M. carried out the experiments and wrote the main manuscript text. Y.H., W.L., F.Z., B.X., Z.Z., S.C., M.W. checked the data and figures. Q.W. supervised the whole project and revised the manuscript. All authors reviewed the manuscript.

Data Availability No datasets were generated or analysed during the current study.

Declarations

Competing Interests The authors declare no competing interests.

References

Adham Ahmed RC, Willneff E, Ritchie H,Peter, Myers H, Zhang (2010) Synthesis of uniform porous silica microspheres with hydrophilic polymer as stabilizing agent. Ind. Eng. Chem. Res. 49: 602–608. https://doi.org/10.1021/ie901213v

Adnan M, Xiao B, Xiao P et al (2022) Research progress on heavy metals pollution in the soil of smelting sites in China. Toxics 10:231. https://doi.org/10.3390/toxics10050231

Ahmad Z, Li Y, Huang C et al (2021) Underwater suspended bifunctionalized polyethyleneimine-based sponge for selective removal of anionic pollutants from aqueous solution. J Hazard Mater 412:125284. https://doi.org/10.1016/j.jhazmat.2021.125284

An F, Wu R, Li M et al (2017) Adsorption of heavy metal ions by iminodiacetic acid functionalized D301 resin: kinetics, isotherms and thermodynamics. Reactive Funct Polym 118:42–50. https://doi.org/10.1016/j.reactfunctpolym.2017.07.005

An Y, Zheng H, Yu Z et al (2020) Functioned hollow glass microsphere as a self-floating adsorbent: Rapid and high-efficient removal of anionic dye. J Hazard Mater 381:120971. https://doi.org/10.1016/j.jhazmat.2019.120971

Awual MR (2019) A facile composite material for enhanced cadmium(II) ion capturing from wastewater. J Environ Chem Eng 7:103378. https://doi.org/10.1016/j.jece.2019.103378

Awual MR, Rahman IMM, Yaita T et al (2014) pH dependent cu(II) and pd(II) ions detection and removal from aqueous media by an efficient mesoporous adsorbent. Chem Eng J 236:100–109. https://doi.org/10.1016/j.cej.2013.09.083

Awual MR, Hasan MM, Iqbal J et al (2020) Ligand based sustainable composite material for sensitive nickel(II) capturing in aqueous media. J Environ Chem Eng 8:103591. https://doi.org/10.1016/j.jece.2019.103591

Benalia MC, Youcef L, Bouaziz MG et al (2021) Removal of heavy metals from industrial wastewater by chemical precipitation: mechanisms and sludge characterization. Arab J Sci Eng 47:5587–5599. https://doi.org/10.1007/s13369-021-05525-7

Beniamino Y, Cenni V, Piccioli M et al (2022) The ni(II)-binding activity of the intrinsically disordered region of human NDRG1, a protein involved in cancer development. Biomolecules 12:1272. https://doi.org/10.3390/biom12091272

Boumediene M, Benaissa H, George B et al (2015) Characterization of two cellulosic waste materials (orange and almond peels) and their use for the removal of methylene blue from aqueous solutions. Maderas-Ciencia Y Tecnologia 17:69–84. https://doi.org/10.4067/s0718-221x2015005000008

Cai W, Dionysiou DD, Fu F et al (2020) CTAB–intercalated molybdenum disulfide nanosheets for enhanced simultaneous removal of cr(VI) and ni(II) from aqueous solutions. J Hazard Mater 396:122728. https://doi.org/10.1016/j.jhazmat.2020.122728

Chen YY, Yu SH, Jiang HF et al (2018) Performance and mechanism of simultaneous removal of cd(II) and Congo Red from aqueous solution by hierarchical vaterite spherulites. Appl Surf Sci 444:224–234. https://doi.org/10.1016/j.apsusc.2018.03.081

Damiri F, Andra S, Kommineni N et al (2022) Recent advances in adsorptive nanocomposite membranes for heavy metals ion removal from contaminated water. Compr Rev Mater 15:5392. https://doi.org/10.3390/ma15155392

Dawodu FA, Akpomie KG (2014) Simultaneous adsorption of Ni(II) and mn(II) ions from aqueous solution unto a Nigerian kaolinite clay. J Mater Res Technology-Jmr&T 3:129–141. https://doi.org/10.1016/j.jmrt.2014.03.002

Debnath S, Ghosh UC (2009) Nanostructured hydrous titanium(IV) oxide: synthesis, characterization and ni(II) adsorption behavior. Chem Eng J 152:480–491. https://doi.org/10.1016/j.cej.2009.05.021

Dou J, Gan D, Huang Q et al (2019a) Functionalization of carbon nanotubes with chitosan based on MALI multicomponent reaction for Cu^{2+} removal. Int J Biol Macromol 136:476–485. https://doi.org/10.1016/j.ijbiomac.2019.06.112

Dou J, Huang Q, Huang H et al (2019b) Mussel-inspired preparation of layered double hydroxides based Polymer composites for removal of copper ions. J Colloid Interface Sci 533:416–427. https://doi.org/10.1016/j.jcis.2018.08.064

Gong J, Feng J, Liu J et al (2014) Catalytic carbonization of polypropylene into cup-stacked carbon nanotubes with high performances in adsorption of heavy metallic ions and organic dyes. Chem Eng J 248:27–40. https://doi.org/10.1016/j.cej.2014.01.107

Guo R, Bao Y, Kang Q et al (2022a) Solvent-controlled synthesis and photocatalytic activity of hollow TiO_2 microspheres prepared by the solvothermal method. Colloids Surf a 633:127931. https://doi.org/10.1016/j.colsurfa.2021.127931

Guo S, Liu Y, Zhang W et al (2022b) N-doped carbon fibers in situ prepared by hydrothermal carbonization of Camellia sinensis branches waste for efficient removal of heavy metal ions. Environ Sci Pollut Res 29:88951–88961. https://doi.org/10.1007/s11356-022-21923-2

Hu X, Yan L, Wang Y et al (2021) Ion-imprinted sponge produced by ice template-assisted freeze drying of salecan and graphene oxide nanosheets for highly selective adsorption of mercury (II) ion. Carbohydr Polym 258:117622. https://doi.org/10.1016/j.carbpol.2021.117622

Islam MA, Awual MR, Angove MJ (2019) A review on nickel(II) adsorption in single and binary component systems and future path. J Environ Chem Eng 7:103305. https://doi.org/10.1016/j.jece.2019.103305

Jin J, Yang L, Chen F et al (2022) Drug delivery system based on nanobubbles. Interdisciplinary Mater 1:471–494. https://doi.org/10.1002/idm2.12050

Karim MR, Aijaz MO, Alharth NH et al (2019) Composite nanofibers membranes of poly(vinyl alcohol)/chitosan for selective lead(II) and cadmium(II) ions removal from wastewater. Ecotoxicol Environ Saf 169:479–486. https://doi.org/10.1016/j.ecoenv.2018.11.049

Khatun J, Intekhab A, Dhak D (2022) Effect of uncontrolled fertilization and heavy metal toxicity associated with arsenic(as), lead(pb) and cadmium (cd), and possible remediation. Toxicology 477:153274. https://doi.org/10.1016/j.tox.2022.153274

Kusworo TD, Kumoro AC, Aryanti N et al (2021) Removal of organic pollutants from rubber wastewater using hydrophilic nanocomposite rGO-ZnO/PES hybrid membranes. J Environ Chem Eng 9:106421. https://doi.org/10.1016/j.jece.2021.106421

Liang S, Shen L, Zhou C et al (2020) Scalable preparation of hollow ZrO_2 microspheres through a liquid-liquid phase reunion assisted sol-gel method. Ceram Int 46:14188–14194. https://doi.org/10.1016/j.ceramint.2020.02.227

Liu Y, Guo L, Huang H et al (2019) Facile preparation of magnetic composites based on carbon nanotubes: utilization for removal of environmental pollutants. J Colloid Interface Sci 545:8–15. https://doi.org/10.1016/j.jcis.2019.03.009

Liu Y, Li X, Wang Y et al (2020) Hydrothermal synthesis of Au@SnO_2 hierarchical hollow microspheres for ethanol detection. Sens Actuators B 319:128299. https://doi.org/10.1016/j.snb.2020.128299

Liu C, Liu N, Li X et al (2022) Adsorption of cd(II) on mesoporous Al_2O_3 prepared from high-aluminum fly ash. Mater Res Express 9:065502. https://doi.org/10.1088/2053-1591/ac7383

Lv Y, Yang L, Wang J et al (2022) Performance of ultra-high-performance concrete incorporating municipal solid waste incineration fly ash. Case Stud Constr Mater 17:e01155. https://doi.org/10.1016/j.cscm.2022.e01155

Malayoglu U (2018) Removal of heavy metals by biopolymer (chitosan)/nanoclay composites. Sep Sci Technol 53:2741–2749. https://doi.org/10.1080/01496395.2018.1471506

Mao S, Gao M (2021) Functional organoclays for removal of heavy metal ions from water: a review. J Mol Liq 334:116143. https://doi.org/10.1016/j.molliq.2021.116143
Monier M, Ayad DM, Wei Y et al (2010) Adsorption of Cu(II), Co(II), and Ni(II) ions by modified magnetic chitosan chelating resin. J Hazard Mater 177:962–970. https://doi.org/10.1016/j.jhazmat.2010.01.012
Ong DC, Pingul-Ong SMB, Kan C-C et al (2018) Removal of nickel ions from aqueous solutions by manganese dioxide derived from groundwater treatment sludge. J Clean Prod 190:443–451. https://doi.org/10.1016/j.jclepro.2018.04.175
Punia P, Bharti MK, Dhar R et al (2022) Recent advances in detection and removal of heavy metals from contaminated water. ChemBioEng Reviews 9:351–369. https://doi.org/10.1002/cben.202100053
Qiao Y, Li Q, Li Q et al (2022) Lightweight epoxy foams prepared with arranged hollow-glass-microspheres/epoxy hollow spheres. Compos Commun 33:101197. https://doi.org/10.1016/j.coco.2022.101197
Rajurkar NS, Gokarn AN, Dimya K (2011) Adsorption of chromium(III), nickel(II), and copper(II) from aqueous solution by activated alumina. Clean-Soil Air Water 39:767–773. https://doi.org/10.1002/clen.201000273
Razzak SA, Faruque MO, Alsheikh Z et al (2022) A comprehensive review on conventional and biological-driven heavy metals removal from industrial wastewater. Environ Adv 7:100168. https://doi.org/10.1016/j.envadv.2022.100168
Rostamian R, Najafi M, Rafati AA (2011) Synthesis and characterization of thiol-functionalized silica nano hollow sphere as a novel adsorbent for removal of poisonous heavy metal ions from water: kinetics, isotherms and error analysis. Chem Eng J 171:1004–1011. https://doi.org/10.1016/j.cej.2011.04.051
Salihi EÇ, Wang J, Coleman DJL et al (2016) Enhanced removal of nickel(II) ions from aqueous solutions by SDS-functionalized graphene oxide. Sep Sci Technol 51:1317–1327. https://doi.org/10.1080/01496395.2016.1162172
Salman MS, Sheikh MC, Hasan MM et al (2023) Chitosan-coated cotton fiber composite for efficient toxic dye encapsulation from aqueous media. Appl Surf Sci 622:157008. https://doi.org/10.1016/j.apsusc.2023.157008
Samad SA, Arafat A, Ferrari R et al (2021) Adsorption studies and effect of heat treatment on porous glass microspheres. Int J Appl Glass Sci 13:63–81. https://doi.org/10.1111/ijag.16352
Sheikh MC, Hasan MM, Hasan MN et al (2023) Toxic cadmium(II) monitoring and removal from aqueous solution using ligand-based facial composite adsorbent. J Mol Liq 389:122854. https://doi.org/10.1016/j.molliq.2023.122854
Song P, Xu D, Yue J et al (2022) Recent advances in soil remediation technology for heavy metal contaminated sites: a critical review. Sci Total Environ 838:156417. https://doi.org/10.1016/j.scitotenv.2022.156417
Tang Y, Liang S, Wang J et al (2013) Amino-functionalized core-shell magnetic mesoporous composite microspheres for pb(II) and cd(II) removal. J Environ Sci 25:830–837. https://doi.org/10.1016/s1001-0742(12)60141-7
Tang T, Han C, Deng J et al (2022) Controllable preparation of thio-functionalized composite polysilsesquioxane microspheres in a microreaction system. Adv Powder Technol 33:103578. https://doi.org/10.1016/j.apt.2022.103578
Thévenod F, Lee W-K (2013) Toxicology of cadmium and its damage to mammalian organs: Cadmium: From Toxicity to Essentiality (ed., pp. 415–490
Velusamy S, Roy A, Sundaram S et al (2021) A review on heavy metal ions and containing dyes removal through graphene oxide-based adsorption strategies for textile wastewater treatment. Chem Record 21:1570–1610. https://doi.org/10.1002/tcr.202000153
Vereshchagina TA, Kutikhina EA, Chernykh YY et al (2018) One-step immobilization of cesium and strontium from alkaline solutions via a facile hydrothermal route. J Nucl Mater 510:243–255. https://doi.org/10.1016/j.jnucmat.2018.08.015
Waliullah RM, Rehan AI, Awual ME et al (2023) Optimization of toxic dye removal from contaminated water using chitosan-grafted novel nanocomposite adsorbent. J Mol Liq 388:122763. https://doi.org/10.1016/j.molliq.2023.122763
Wang Y, Yao L, Xu L et al (2021) One-step solvothermal synthesis of hierarchical WO3 hollow microspheres with excellent NO gas sensing properties. Mater Lett 302:130460. https://doi.org/10.1016/j.matlet.2021.130460
Wang L, Tan X, Zhu Q et al (2022a) The universality applications of MoS_2@MnS heterojunction hollow microspheres for univalence organic or multivalence aqueous electrolyte energy storage device. J Power Sources 518:230747. https://doi.org/10.1016/j.jpowsour.2021.230747
Wang Y, Chen F, Han W et al (2022b) Carbothermal synthesis of zirconium carbide hollow microspheres from polyzirconoxane and phenolic resin by spray drying. Ceram Int 48:2793–2801. https://doi.org/10.1016/j.ceramint.2021.10.068

Wu J-M, Li M, Liu S-S et al (2021) Selective laser sintering of porous Al_2O_3-based ceramics using both Al_2O_3 and SiO_2 poly-hollow microspheres as raw materials. Ceram Int 47:15313–15318. https://doi.org/10.1016/j.ceramint.2021.02.096

Wu H, Jiang A, Li M et al (2022) Preparation of core-shell-structured RDX@PVDF microspheres with improved thermal stability and decreased mechanical sensitivity. Polymers 14:4262. https://doi.org/10.3390/polym14204262

Xiong C, Wang W, Tan F et al (2015) Investigation on the efficiency and mechanism of cd(II) and pb(II) removal from aqueous solutions using MgO nanoparticles. J Hazard Mater 299:664–674. https://doi.org/10.1016/j.jhazmat.2015.08.008

Xu P, Nan Z, Zhu A et al (2017) A facile method for preparation of hollow mesoporous silica sphere and its application. Mater Lett 205:20–23. https://doi.org/10.1016/j.matlet.2017.06.045

Yan S, Zhang F, Wang L et al (2019) A green and low-cost hollow gangue microsphere/geopolymer adsorbent for the effective removal of heavy metals from wastewaters. J Environ Manage 246:174–183. https://doi.org/10.1016/j.jenvman.2019.05.120

Yang W, Tang Q, Wei J et al (2016) Enhanced removal of cd(II) and pb(II) by composites of mesoporous carbon stabilized alumina. Appl Surf Sci 369:215–223. https://doi.org/10.1016/j.apsusc.2016.01.151

Yuan X, Luo F, Chen X et al (2022) Effective cu(II) ions adsorption from aqueous solutions using low grade oolitic hematite tailing with phosphorus: response surface methodology. Desalination Water Treat 265:57–70. https://doi.org/10.5004/dwt.2022.28594

Yun-Kai Lu X-PY (2004) An imprinted organic inorganic hybrid sorbent for selective separation of cadmium from aqueous solution. Anal Chem 76:453–457. https://doi.org/10.1021/ac0347718

Zhang X, Wang X (2015) Adsorption and desorption of nickel(II) iions from aqueous solution by a lignocellulose/montmorillonite nanocomposite. PLoS ONE 10:e0117077. https://doi.org/10.1371/journal.pone.0117077

Zhang F, Wang B, He S et al (2014) Preparation of graphene-oxide/polyamidoamine dendrimers and their adsorption properties toward some heavy metal ions. J Chem Eng Data 59:1719–1726. https://doi.org/10.1021/je500219e